

FRAP: Faithful and Realistic Text-to-Image Generation with Adaptive Prompt Weighting

Liyao Jiang^{1,2}, Negar Hassanpour², Mohammad Salameh²,
Mohan Sai Singamsetti², Fengyu Sun³, Wei Lu³, Di Niu¹

¹Dept. ECE, University of Alberta. ²Huawei Technologies Canada. ³Huawei Kirin Solution, China.
{liyao1, dniu}@ualberta.ca, {negar.hassanpour2, mohammad.salameh, mohan.sai.singamsetti}@huawei.com
{sunfengyu, robin.luwei}@hisilicon.com

Abstract

Text-to-image (T2I) diffusion models have demonstrated impressive capabilities in generating high-quality images given a text prompt. However, ensuring the prompt-image alignment remains a considerable challenge, i.e., generating images that faithfully align with the prompt’s semantics. Recent works attempt to improve the faithfulness by optimizing the latent code, which potentially could cause the latent code to go out-of-distribution and thus produce unrealistic images. In this paper, we propose FRAP, a simple, yet effective approach based on adaptively adjusting the per-token prompt weights to improve prompt-image alignment and authenticity of the generated images. We design an online algorithm to adaptively update each token’s weight coefficient, which is achieved by minimizing a unified objective function that encourages object presence and the binding of object-modifier pairs. Through extensive evaluations, we show FRAP generates images with significantly higher prompt-image alignment to prompts from complex datasets, while having a lower average latency compared to recent latent code optimization methods, e.g., 4 seconds faster than D&B on the COCO-Subject dataset. Furthermore, through visual comparisons and evaluation on the CLIP-IQA-Real metric, we show that FRAP not only improves prompt-image alignment but also generates more authentic images with realistic appearances. We also explore combining FRAP with prompt rewriting LLM to recover their degraded prompt-image alignment, where we observe improvements in both prompt-image alignment and image quality.

Introduction

Recent text-to-image (T2I) diffusion models (Rombach et al. 2022; Chang et al. 2023; Kang et al. 2023) have demonstrated impressive capabilities in synthesizing photo-realistic images given a text prompt. Faithfulness and authenticity are among the most important aspects to assess the quality of AI generated content, where faithfulness is evaluated by prompt-image alignment metrics (Radford et al. 2021; Li et al. 2022; Chefer et al. 2023) and authenticity reflects how realistic the image appears and is usually evaluated by image quality assessment metrics (Wang, Chan, and Loy 2023; Wu et al. 2023). While recent T2I diffusion models are capable of generating realistic images with high aesthetic quality, it has been shown (Chefer et al. 2023; Feng et al. 2022; Wang et al. 2022) that the AI generated images

may not always faithfully align with the semantics of the given text prompt. One typical issue that compromises the model’s ability to align with the given prompt is catastrophic neglect (Chefer et al. 2023), where one or more objects are missing in the generated image. Another common alignment issue is incorrect modifier binding (Li et al. 2023), where the modifiers, e.g., color, texture, etc., are either bound to the wrong object mentioned in the prompt or ignored. The generation can also result in an unrealistic mix or hybrid of different objects.

To improve prompt-image alignment, Attend & Excite (A&E) (Chefer et al. 2023) introduces the Generative Semantic Nursing (GSN) method, which iteratively adjusts the latent code throughout the reverse generative process (RGP) by optimizing a loss function defined on cross-attention (CA) maps to improve attention to under-attended objects. Similarly, Divide & Bind (D&B) (Li et al. 2023) uses GSN to improve the binding between objects and modifiers, by designing an optimization objective that aligns the attention of objects and their related modifiers. Although GSN can alleviate the semantic alignment issues, yet the iterative updates to latent code could potentially drive the latent code out-of-distribution (OOD), resulting in less realistic images being generated. In addition, several recent works investigate prompt optimization (Hao et al. 2023; Valerio et al. 2023; Mañas et al. 2024), which aims to improve image aesthetics while trying to maintain the prompt-image alignment, by rewriting the user-provided text prompt with a large language model (LLM). Despite improvements on image aesthetic quality, Mañas et al. (2024) show that rewriting prompts primarily for aesthetics enhancement could harm the semantic alignment between the image and prompt. Therefore, it remains a significant challenge to generate images to ensure prompt-image alignment while achieving realistic appearance and high aesthetic quality.

In this paper, we introduce Faithful and Realistic Text-to-Image Generation with Adaptive Prompt Weighting (FRAP), which adaptively adjusts the per-token prompt weighting throughout the RGP of a diffusion model to improve the prompt-image alignment while still generating high-quality images with realistic appearance. Unlike the conventional manual prompt weighting techniques (Face 2023a; Stewart 2023), we design an online optimization algorithm which is performed during inference and updates

each token’s weight coefficient in the prompt to adaptively emphasize or de-emphasize certain tokens at different time-steps, by minimizing a unified objective function defined based on the cross-attention maps to strengthen the presence of the prompted object and encourage modifier binding to objects. Since we optimize each prompt token’s weight coefficient, our approach avoids the above-mentioned out-of-distribution issue associated with directly modifying the latent code. Furthermore, we also introduce a novel usage of FRAP by combining it with LLM-based prompt optimizer to achieve outstanding enhancement to both prompt alignment and generation quality.

We extensively evaluate the faithfulness, authenticity and aesthetic quality of FRAP-generated images via prompt-image alignment metrics and a range of image quality assessment metrics and make the following observations:

- We observe that FRAP achieves significantly higher faithfulness than recent methods on all prompt-image alignment metrics on the Color-Obj-Scene, COCO-Subject, and COCO-Attribute datasets (Li et al. 2023) which contain complex and challenging prompts, while remaining on par with these methods on simple datasets with prompts created from templates. In the meantime, the images generated by FRAP demonstrate higher authenticity with more realistic appearance in terms of the CLIP-IQA-Real measure (Wang, Chan, and Loy 2023).
- While improving prompt-image alignment and generating more realistic and authentic images, our method requires lower average inference latency (e.g., 4 seconds faster than D&B on the COCO-Subject dataset) and lower number of UNet calls by not making repeated calls of UNet at each time-step during inference, in contrast to the recent GSN methods (Chefer et al. 2023; Li et al. 2023) which calls the UNet multiple times in a refinement loop at each time-step, especially on datasets with complex prompts that require many repeated calls.
- We observe that although the LLM prompt rewriting method Promptist (Hao et al. 2023) improves the image aesthetic quality, it could harm the semantic alignment between the image and prompt. Moreover, our adaptive prompt weighting approach can be easily integrated with recent prompt rewrite methods (Hao et al. 2023; Valerio et al. 2023; Mañas et al. 2024). We explore applying FRAP to the rewritten prompts of Promptist to recover their degraded prompt-image alignment, where we observe improvements in both the prompt-image alignment and image quality.

Preliminaries

Stable Diffusion (SD)

We implement our approach based on the open-source SOTA T2I latent diffusion model SD (Rombach et al. 2022). Unlike traditional diffusion models (such as (Sohl-Dickstein et al. 2015; Ho, Jain, and Abbeel 2020; Song, Meng, and Ermon 2020)) that work in the pixel space, SD operates in an autoencoder’s latent space, which significantly reduces the amount of compute resources required. SD is composed of

several components, including a Variational Auto-Encoder (VAE) (Kingma and Welling 2013; Rezende, Mohamed, and Wierstra 2014)¹, a UNet (Ronneberger, Fischer, and Brox 2015) that operates in the latent space and serves as the backbone for image generation, and a Text Encoder that is used to obtain embeddings from the text prompt.

UNet. For training the UNet, the forward diffusion process (Ho, Jain, and Abbeel 2020) is used to collect a training dataset. Noise ϵ is gradually added to the original latent z_0 over T time-steps², and the info corresponding to a subset of time-steps t is recorded in a form of $\{t, z_t, \epsilon_t\}$. Rombach et al. (2022) trained a UNet (Ronneberger, Fischer, and Brox 2015) denoiser, parameterized by θ , to predict the added noise ϵ_t conditioned on the latent code z_t , the time-step t , and the text embedding c from the text encoder:

$$\mathcal{L}_{\text{train}} = \mathbb{E}_{z \sim \mathcal{E}(x), y, \epsilon \sim \mathcal{N}(0,1)} \left[\|\epsilon - \epsilon_{\theta}(z_t, t, c)\|_2^2 \right]. \quad (1)$$

To generate novel images conditioned on text prompt, the already-trained UNet is called to sequentially denoise a latent code sampled from the unit Gaussian distribution $z_T \sim \mathcal{N}(0, 1)$ and conditioned on the text embedding c , by traversing back through T time-steps following the RGP. The denoising process results in producing a clean final latent code z_0 , which is passed to the VAE’s decoder to obtain the respective generated image $\mathcal{I} = \mathcal{D}(z_0)$.

Cross-Attention (CA). The CA unit is responsible for injecting the prompt information into the model. A CA map at time-step t is denoted by A_t , having a $P \times P \times N$ tensor size, where P is the spatial dimension of the intermediate feature map and N is the number of prompt tokens. The CA layer weights project the text embedding c into keys K and values V , while queries Q are mapped from the intermediate feature map of the UNet. Subsequently, the CA map A_t is calculated as $A_t = \text{Softmax}(\frac{QK^T}{\sqrt{d}})$.³ We represent the CA map for token n by $A_t^n = A_t[:, :, n]$. We utilize the same Gaussian filter G from (Chefer et al. 2023) to smooth the CA map (i.e., $G(A_t^n)$) for each token. Smoothing the CA maps ensures that the influence of neighboring patches is also reflected in the probability of each patch.

Text Encoder. Conditioned on the text prompt y , the CLIP (Radford et al. 2021) text encoder produces an $N \times H$ text embedding tensor c^y , where $c^y = \text{CLIP}(y) = [c^{y,1}, c^{y,2}, \dots, c^{y,N}]$, N denotes the number of tokens, and H is dimension of the text embedding. To satisfy the requirements for the classifier-free guidance (CFG) (Ho and Salimans 2022) approach, an unconditional text embedding is also generated from the null text \emptyset , where $c^{\emptyset} = \text{CLIP}(\emptyset) = [c^{\emptyset,1}, c^{\emptyset,2}, \dots, c^{\emptyset,N}]$. The conditional token embedding for token n is denoted as $c^{y,n} \in \mathbb{R}^H$ and the unconditional token embedding for token n is denoted as $c^{\emptyset,n} \in \mathbb{R}^H$.

¹The VAE encoder \mathcal{E} maps an input image x into its spatial latent representation $z = \mathcal{E}(x)$, while the decoder \mathcal{D} attempts to reconstruct the same image from z such that $\mathcal{D}(\mathcal{E}(x)) \approx x$.

²Often, T is chosen to be a large number (e.g., 1000) such that z_T is close to the unit Gaussian noise.

³As such, $A_t[i, j, :]$ defines a probability distribution over the tokens.

Prompt Weighting

Prompt weighting (Face 2023a; Stewart 2023) is a popular technique among SD art creators for obtaining more control over the image generation process. Users can manually specify per-token weight coefficients $\phi = [\phi^1, \phi^2, \dots, \phi^N]$ to emphasize or de-emphasize the semantics behind each token. Prompt weighting obtains a weighted text embedding \tilde{c}^y by interpolating between the conditional text embedding c^y and the unconditional text embedding c^\emptyset with the weight coefficients ϕ as follows:

$$\tilde{c}^y(\phi, c^y, c^\emptyset) = \phi \odot c^y + (1 - \phi) \odot c^\emptyset, \quad (2)$$

where \odot denotes, e.g., multiplication of each scalar ϕ^i by token i 's embedding vector $c^{y,i}$.

The SD model adopts the CFG (Ho and Salimans 2022) approach to control the strength of conditional information on the generated image. This strength is controlled with a guidance scale β . With the prompt weighted text embedding \tilde{c}^y , CFG updates the UNet's predicted noise as follows:

$$\tilde{\epsilon}_\theta(z_t, t, c) = \beta \epsilon_\theta(z_t, t, \tilde{c}^y) + (1 - \beta) \epsilon_\theta(z_t, t, c^\emptyset). \quad (3)$$

The manual prompt weighting technique (Face 2023a; Stewart 2023) uses fixed weight coefficients throughout the entire RGP. Moreover, for every single prompt, the users must manually determine the weight coefficients through expert knowledge.⁴

Related works

T2I generation has been most successful with the recent advancement in diffusion models (Sohl-Dickstein et al. 2015; Ho, Jain, and Abbeel 2020). These include large-scale models such as Stable Diffusion (SD) (Rombach et al. 2022), Imagen (Saharia et al. 2022), MidJourney (Midjourney.com 2023), and Dall-E 2 (Ramesh et al. 2022). Although these SOTA models have adopted methods such as classifier guidance (CG) (Dhariwal and Nichol 2021) and CFG (Ho and Salimans 2022), it remains a challenge for them to enforce proper alignment with some prompt scenarios (Chefer et al. 2023; Feng et al. 2022; Wang et al. 2022; Marcus, Davis, and Aaronson 2022). Several engineering techniques have been developed to partially address this shortcoming (Liu and Chilton 2022; Marcus, Davis, and Aaronson 2022; Witteveen and Andrews 2022).

A recent line of work attempts to automate this task by developing methods for training-free improvement of the semantics compliance of SD, which is an open-sourced SOTA model. In the remainder of this section, we describe the most prominent related works in the literature and touch on their potential limitations.

StructureDiffusion (Feng et al. 2022) used a language model to obtain hierarchical structures from the prompt in the form of noun phrases. They then used the average of the respective CA maps (Hertz et al. 2022) as the output of the CA unit. This method, however, is limited in terms of

⁴The manual prompt weighting library (Stewart 2023) suggests a bounded range of $\phi \in [0.5, 1.5]$, since too large or too small of a weighting coefficient has been empirically shown to create low-quality results.

its ability to generate images that diverge significantly from those produced by SD (Rombach et al. 2022).

Attend & Excite (A&E) (Chefer et al. 2023) introduced the novel concept of GSN, which refers to manipulating the latent codes to guide the RGP towards improving the image alignment with the prompt. They proposed a loss function based on the CA maps to update the latent codes at each time-step. However, their loss function does not explicitly consider the modifier binding issue. Moreover, it only considers a point estimate (i.e., the highest pixel value among all CA maps of noun objects), making it susceptible to having robustness issues.

Divide & Bind (D&B) (Li et al. 2023) adopted the GSN idea (Chefer et al. 2023), but proposed a novel composite loss function that addresses both catastrophic neglect with a Total Variation (TV) loss, as well as the modifier binding issue with a Jensen Shannon Divergence (JSD) loss.

SynGen (Rassin et al. 2023) employed a language model (spaCy's transformer-based dependency parser (Honnibal and Montani 2017)) to syntactically analyze the prompt. This was to first identify entities and their modifiers, and then use CA maps to create an objective that encourages the modifier binding only. As a result, if the latent code misses an object for some reason, their binding-only loss cannot compensate for this error.

Method

Prior works (Chefer et al. 2023; Li et al. 2023) improve the semantic guidance in SD by optimizing the latent code during inference. These methods demonstrate excellent capability in addressing semantic compliance issues. However, the latent code could go out-of-distribution (OOD) after several iterative updates, which could lead to generation of unrealistic images.

To address this issue, we propose a simple, yet effective approach based on the prompt weighting technique that improves faithfulness while maintaining the realistic appearance of generated images. Unlike the manual approach, FRAP adaptively updates the weight coefficients of different text tokens during the RGP to emphasize or de-emphasize certain tokens in order to facilitate improving faithfulness. The weights are guided by our unified objective function defined on the CA maps, strengthening the object presence and encouraging object-modifier binding.

The following subsections describe our proposed unified objective function and adaptive prompt weighting method. The overview of FRAP is illustrated in Fig. 1. In the supplementary materials, we present the overall algorithm and implementation details of our proposed method.

Unified Objective

We propose a novel objective function \mathcal{L} , defined on the CA maps, to address improving the alignment of a generated image with the prompt. This unified objective function is used as the loss for on-the-fly optimization of the adaptive prompt weight parameters. Our proposed unified objective function \mathcal{L}_t at time-step t consists of two terms: (i) the object presence loss $\mathcal{L}_{\text{presence},t}$ and (ii) the object-modifier binding loss

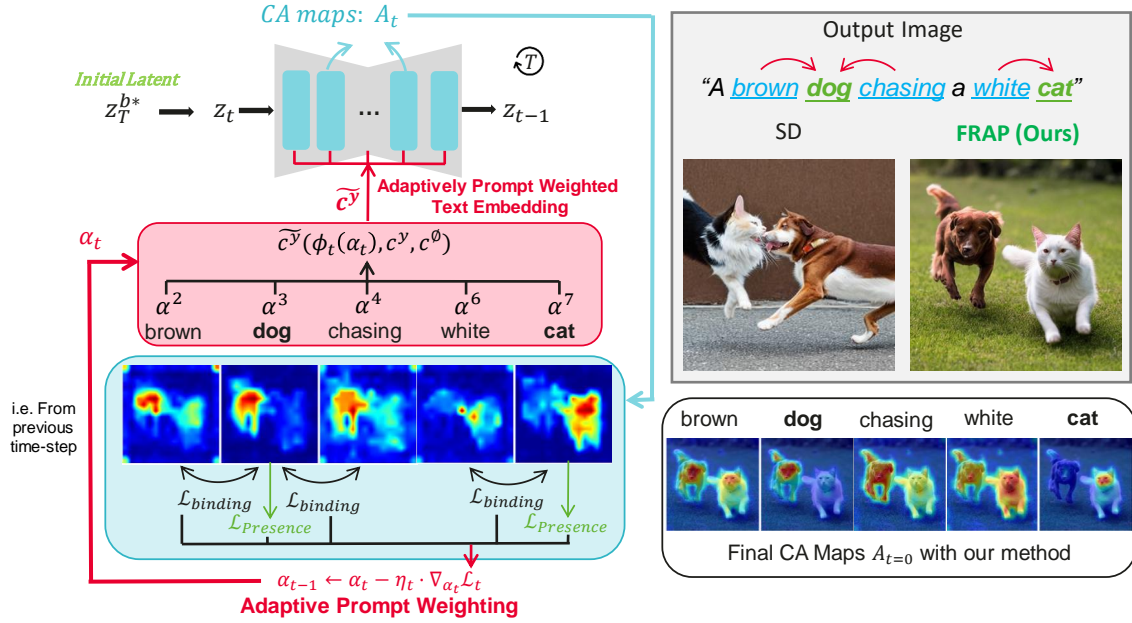


Figure 1: **Method overview.** We perform adaptive updates to the per-token prompt weight coefficients to improve faithfulness. The updates are guided by our unified loss function, defined on the CA maps, which strengthens object presence and encourages object-modifier binding. FRAP is capable of correctly generating every object along with accurate object-modifier bindings.

$\mathcal{L}_{\text{binding},t}$. The overall objective function is defined as:

$$\mathcal{L}_t = \mathcal{L}_{\text{presence},t} - \lambda \mathcal{L}_{\text{binding},t}, \quad (4)$$

where λ is a hyperparameter.

The object presence loss is defined on the set of object tokens S in the text prompt to reinforce the presence of each object $s \in S$ in the generated image to prevent neglect or generating hybrid creatures. The object-modifier binding loss is defined on the set of object-modifier token pairs $(s, r) \in P(s, R_s)$ for $s \in S$, to encourage the correct binding of each object token s and each of its related modifier token $r \in R_s$. To automate the manual identification of object and modifier tokens in (Chefer et al. 2023; Li et al. 2023), we follow SynGen (Rassin et al. 2023) and use the spaCy (Honibal and Montani 2017) language parser to extract the object and modifier tokens as explained in the supplementary materials.

Object Presence Loss. Our object presence loss aims to enhance the significance of each object token $s \in S$. We achieve this by maximizing the largest activation value of the Gaussian smoothed CA map $G(A_t^s)$ for each object token. We define the loss for s at time-step t as:

$$\mathcal{L}_{\text{presence},t}^s = 1 - \max(G(A_t^s)). \quad (5)$$

Object-Modifier Binding Loss. The loss function for object-modifier binding aims to ensure that each object is correctly aligned with its corresponding modifier tokens in terms of spatial positioning. To achieve this, the probability densities of each pair $(s, r) \in P(s, R_s)$ should overlap as

much as possible. We define the binding loss as follows:

$$\mathcal{L}_{\text{binding},t}^{s,r} = \frac{1}{P^2} \sum_{\text{pixels}} \left(\min \left(\Pr(G(A_t^s)), \Pr(G_a(A_t^r)) \right) \right), \quad (6)$$

where P is the spatial dimension of the CA map, $G_a(A_t^r)$ denotes the aligned smoothed CA map of the token r according to token s following (Li et al. 2023), and $\Pr(G(A_t^s))$ is the normalized discrete probability distribution of the smoothed CA map of token s . This distribution is obtained by applying Softmax over all pixels of the respective CA map. We apply the same process to get $\Pr(G_a(A_t^r))$.

Next, as shown in Eq. (4), we maximize this minimum overlap between the two discrete probability distributions in a minimax fashion.⁵ The minimax approach aims to ensure a robust match between the CA maps. This is particularly useful for representing small objects in a scene. Moreover, it is less susceptible to the influence of outliers compared to divergence methods such as JSD, which is beneficial in handling noisy and uncertain CA maps.

Overall Loss. We calculate the total presence loss as the mean of per-token object presence loss for all object tokens $s \in S$:

$$\mathcal{L}_{\text{presence},t} = \frac{1}{|S|} \sum_{s \in S} \mathcal{L}_{\text{presence},t}^s. \quad (7)$$

For the total object-modifier binding loss, we compute it as the mean of all pairwise object-modifier binding loss

⁵Note the negative sign for $\mathcal{L}_{\text{binding},t}$ in Eq. (4), which results in maximizing the minimum overlap.

$\mathcal{L}_{\text{binding},t}^{s,r}$ for all $(s, r) \in P(S, R)$:

$$\mathcal{L}_{\text{binding},t} = \frac{1}{|P(S, R)|} \sum_{(s,r) \in P(S,R)} \mathcal{L}_{\text{binding},t}^{s,r} \quad (8)$$

Finally, we calculate the total overall loss \mathcal{L}_t at time-step t according to Eq. (4).

Note that our per-token presence loss in Eq. (5) is the same as A&E’s (Chefer et al. 2023). However, different from A&E, we use the mean among all objects as the total object presence loss instead of only using the loss from the most neglected token with the lowest max activation. This enhances the presence of *all* objects instead of a single one, which is expected to be essential for complex prompts. We ablate our loss design in the supplementary materials.

Adaptive Prompt Weighting

Different from the manual prompt weighting (Face 2023a; Stewart 2023), we propose FRAP, an adaptive prompt weighting method, to update the weight coefficients during the RGP automatically. We update the per-token weight coefficients ϕ after each time-step t according to our unified loss objective \mathcal{L}_t (see Eq. (4)) defined on the internal feedback from the CA maps. Our approach determines the per-token weights automatically and appropriately for each token to encourage the SD (Rombach et al. 2022) model to generate images that are faithful to the semantics and have a realistic appearance.

In adaptive prompt weighting, we define learnable per-token weight parameters $\alpha = [\alpha^1, \alpha^2, \dots, \alpha^N]$ and use the Sigmoid function σ to obtain the weight values ϕ bounded within $[\phi_{LB}, \phi_{UB}]$ via:

$$\phi = \phi_{LB} + (\phi_{UB} - \phi_{LB})\sigma(\alpha). \quad (9)$$

During the RGP, we perform on-the-fly optimization to the weight parameters α_t according to the gradient $\nabla_{\alpha_t} \mathcal{L}_t$ after each time-step t . Then, we use the updated weight parameters α_{t-1} to strengthen the object presence and encourage better object-modifier binding in the next time-step $t - 1$:

$$\alpha_{t-1} = \alpha_t - \eta_t \cdot \nabla_{\alpha_t} \mathcal{L}_t, \quad (10)$$

where η_t is a scalar step-size for the gradient update. We obtain the bounded next time-step per-token weight coefficients ϕ_{t-1} from α_{t-1} using Eq. (9).

At time-step $t = T$, we initialize $\alpha_T = \vec{0}$ so we start from a trivial weighting of $\phi_T = \vec{1}$ (equivalent to the standard SD with no prompt weighting). Then, our on-the-fly optimization will gradually adjust the weight coefficients to improve alignment with the prompt. This optimization step takes place during inference with no additional overhead for model training. We only perform one UNet inference call at each time-step, and we use the weight parameter α_t obtained from the optimization in the previous time-step $t + 1$ to get the current weight coefficient ϕ_t . Thus, our adaptive prompt weighting process keeps the same number of UNet calls as the standard SD (Rombach et al. 2022). In contrast, other methods such as A&E (Chefer et al. 2023) and D&B (Li et al. 2023) perform several optimization refinement steps at each time-step.

Experiments

In this section, we provide quantitative evaluation and visual comparisons of the effectiveness of FRAP in terms of prompt-image alignment, image quality assessment. We also assess the efficiency of FRAP. In addition, we apply FRAP to the recent prompt rewrite method. In the supplementary materials, we present an ablation study on design choices of FRAP, including a comparison to alternative loss functions. Additionally, we perform evaluations on additional model, baselines, and even larger datasets in the supplementary materials. Moreover, we provide additional visual comparisons and human evaluations in the supplementary materials.

Experimental Settings. We compare our results to SD (Rombach et al. 2022) and to recent methods A&E (Chefer et al. 2023) and D&B (Li et al. 2023). All baselines and our approach are evaluated based on the SDv1.5 (Rombach et al. 2022; Face 2023b) model to align with D&B (Li et al. 2023).⁶ We evaluate on three *Simple*, manually crafted prompt datasets from A&E: Animal-Animal (S-AA), Color-Object (S-CO), and Animal-Object (S-AO); and five *Complex* datasets from D&B: Animal-Scene (C-AS), Color-Object-Scene (C-COS), Multi-Object (C-MO), COCO-Subject (C-CS), and COCO-Attribute (C-CA). For comparing the efficiency of different methods, we measure the end-to-end latency and total number of UNet calls. In the experiments, our method utilizes the unified objective function on early time-step cross-attention maps to efficiently select an initial latent code with decent object presence and object-modifier binding. We obtain the initial latent code by performing 15 initial inference steps on a batch of 4 noisy latent code samples and select one with minimal loss. In the supplementary materials, we further elaborate on the details of the prompt datasets, evaluation metrics, and other experimental settings.

Prompt-Image Alignment and IQA

We use multiple prompt-image alignment metrics and Image Quality Assessment (IQA) metrics to evaluate the performance of various methods and realism of their generated images. Prompt-image alignment metrics include: Text-to-Text Similarity (TTS) (Chefer et al. 2023; Li et al. 2023), Full-prompt Similarity (Full-CLIP) (Chefer et al. 2023), Minimum Object Similarity (MOS) (Chefer et al. 2023). IQA metrics include: Human Preference Score version 2 (HPSv2) (Wu et al. 2023), and CLIP-IQA (Wang, Chan, and Loy 2023). We also report the Real component of CLIP-IQA to explicitly measure how realistic the generated images are. See the supplementary materials for a detailed description of the evaluation metrics.

Due to space constraints, we have placed the detailed performance over 8 datasets and 6 evaluation metrics in the larger Table 4 in the supplementary materials. Summarizing the results here, we observe a tight competition among A&E, D&B, and FRAP across all metrics in datasets with *simple* hand-crafted templates (S-AA, S-CO, and S-AO), while all

⁶Note, however, that FRAP is also applicable to SDXL (Podell et al. 2023) and improves its performance, as evident by our additional experiments (see Table 12 in the supplementary materials).

Table 1: Quantitative comparison of FRAP and other methods on three *complex* datasets Color-Object-Scene, COCO-Subject, and COCO-Attribute. Higher is better (except for latency). Our method is efficient, for instance, FRAP is on average 4 and 5 seconds faster than D&B and A&E respectively, for generating one image on the COCO-Subject dataset.

Dataset	Method	Prompt-Image Alignment			Image Quality Assesment			Latency (s) ↓
		TTS ↑	Full-CLIP ↑	MOS ↑	HPS v2 ↑	CLIP-IQA ↑	CLIP-IQA Real ↑	
Color-Obj-Scene (Li et al. 2023)	SD (Rombach et al. 2022)	0.707	0.366	0.254	0.282	0.675	0.770	8.0
	A&E (Chefer et al. 2023)	0.708	0.376	0.267	0.286	0.675	0.770	17.9
	D&B (Li et al. 2023)	0.719	0.375	0.264	0.286	0.682	0.808	16.7
	FRAP (ours)	0.727	0.381	0.269	0.287	0.676	0.835	14.3
COCO-Subject (Li et al. 2023)	SD (Rombach et al. 2022)	0.829	0.331	0.250	0.278	0.805	0.852	7.9
	A&E (Chefer et al. 2023)	0.829	0.333	0.254	0.277	0.805	0.852	19.1
	D&B (Li et al. 2023)	0.835	0.333	0.253	0.279	0.814	0.862	18.1
	FRAP (ours)	0.837	0.334	0.255	0.279	0.814	0.866	14.0
COCO-Attribute (Li et al. 2023)	SD (Rombach et al. 2022)	0.817	0.347	0.245	0.286	0.703	0.750	8.1
	A&E (Chefer et al. 2023)	0.820	0.353	0.254	0.286	0.703	0.750	15.3
	D&B (Li et al. 2023)	0.821	0.353	0.251	0.288	0.720	0.760	16.7
	FRAP (ours)	0.838	0.358	0.254	0.289	0.725	0.778	13.9

Table 2: Quantitative evaluation of SD, training-based LLM prompt optimization/rewrite method Promptist (Hao et al. 2023), applying FRAP on Promptist rewritten prompt, and FRAP, on the *complex* Color-Object-Scene dataset.

Method	Prompt-Image Alignment			Image Quality Assesment			Lat. (s) ↓
	TTS ↑	Full-CLIP ↑	MOS ↑	HPS v2 ↑	CLIP-IQA ↑	CLIP-IQA Real ↑	
SD	0.707	0.366	0.254	0.282	0.675	0.770	8.0
Promptist	0.666	0.358	0.249	0.279	0.698	0.939	9.2
Promptist+FRAP	0.694	0.377	0.265	0.283	0.702	0.940	15.5
FRAP	0.727	0.381	0.269	0.287	0.676	0.835	14.3

three methods exceed the performance of vanilla SD. This shows that the *simple* datasets may not be sufficient to definitively identify the superior method among the competing options due to the simplicity of the prompts.

We see a clear advantage of FRAP on more challenging *complex* datasets. In Table 1, we observe that FRAP surpasses its competitors in all evaluation metrics on the COCO-Subject and COCO-Attribute datasets, which contain more realistic real-world prompts compared to the manually crafted *simple* datasets. Moreover, in Table 4 in the supplementary materials, we observe that FRAP is consistently best in terms of almost all metrics including TTS, Full-CLIP, HPSv2, and CLIP-IQA-Real on all complex datasets (except for Multi-Object), which demonstrates the ability of FRAP to generate realistic images in various complicated scenarios.

Efficiency Comparisons

Latency values are reported in the last column of Table 1 and also Table 4 in the supplementary materials. FRAP enjoys a lower average latency compared to the recent methods, as it does not rely on costly refinement loops. For instance, FRAP is on average 4 seconds faster than D&B and 5 seconds faster than A&E for generating one image on the C-CS dataset.

Our reported latency measures the average wall-clock time for generating one image on each dataset in seconds with a V100 GPU. Moreover, our method is also more efficient in terms of the number of UNet calls. FRAP consistently use 65 UNet calls which include 15 calls for initial selection steps and 50 calls for adaptive prompt weighting steps. In contrast, A&E and D&B *at least* perform 75 UNet calls which include 25 time-steps with repeated latent code updates each requiring two UNet calls and another 25 normal time-steps each requiring one UNet call. This number will increase for A&E and D&B with more repeated refinement steps needed on more complex prompts at each time-step.

Integration with Prompt Rewrite

In addition to the training-free methods, we also consider the recent training-based prompt optimization method Promptist (Hao et al. 2023) which collect an initial dataset and finetunes an LLM to rewrite user prompts. Note that it requires expensive training, and it needs to run the LLM alongside the T2I diffusion model. In Table 2, our results show that although Promptist improves the image aesthetics, it significantly degrades the prompt-image alignment, demonstrated by the lower alignment scores than SD using the original user prompt. FRAP’s adaptive prompt weighting can easily integrate with prompt rewrite methods and could be applied to the rewritten prompt to recover their degraded prompt-image alignment. By applying FRAP on the rewritten prompt of Promptist, we observed improvements in both the prompt-image alignment and image quality over the Promptist method as shown in Table 2.

Visual Comparisons

Realistic Appearance and Aesthetics. In Fig. 2, we observe that SD (Rombach et al. 2022) ignores one of the objects (e.g., “crown”, “turtle”, “dog”) in all prompts and often incorrectly binds the color modifiers, yet it maintains a good level of realism. Both A&E and D&B generate less realistic images (e.g., “turtle”, “horse”, and “clock” images exhibit cartoonish appearance), likely due to the afore-



Figure 2: **Qualitative comparison (more in supplementary materials)**. Stable Diffusion (Rombach et al. 2022) often exhibits both issues of (i) catastrophic neglect, and (ii) incorrect attribute binding. A&E (Chefer et al. 2023) and D&B (Li et al. 2023) directly modify the latent code to improve faithfulness. However, the latent code could go out-of-distribution after several iterative updates, resulting in lower quality and less realistic images despite improving its semantics. Our FRAP method can generate images that are faithful to the prompt while maintaining a realistic appearance and aesthetics.

mentioned OOD issue. In contrast, FRAP generates images that are more faithful to the prompt, containing all the mentioned objects and well-separated with accurate color bindings (e.g., “clock” and “apple” with correct color bindings instead of a hybrid of two objects as seen for other methods). More importantly, images generated with FRAP maintain a more realistic appearance.

Object Presence and Object-Modifier Binding. Additional visual comparisons are provided in Figs. 5, 6 and 7 in the supplementary materials. In Fig. 5, we observe that SD, A&E, and D&B exhibit object neglect issues on the top four prompts from simple datasets, such as missing “frog”, “bow”, and “dog”. Also, they often generate a hybrid of two objects, such as a “bear” with frog-like feet, a bear-shaped “balloon”, and a toy-like “elephant”. In addition, these images have incorrect color bindings on the prompts. FRAP, however, generates more realistic images and mitigates object neglect, incorrect binding, and hybrid object issues.

Complex Prompts. The bottom four sets of images in Fig. 5 pertain to more complex prompts (C-COS, C-CS, C-CA, and C-MO datasets) which include more objects and more complicated scenes with modifiers. For example, for “a green backpack and a yellow chair on the street, nighttime driving scene”, all three baselines are missing the “yellow chair” or mixing “yellow” with the “road”. On the prompt “a black cat sitting on top of a green bench in a field”, the bench is either neglected or does not have the correct green color. Conversely, FRAP generates images that remain faithful to the prompt on these more complex scenarios.

Conclusions

In this work, we propose FRAP, an adaptive prompt weighting method for improving the prompt-image alignment and authenticity of images generated by diffusion models. We design an online algorithm for adaptively adjusting the per-token prompt weights, which is achieved by minimizing a unified objective function that strengthens object presence and encourages object-modifier binding.

We conduct extensive experiments and demonstrate that FRAP achieves significantly higher faithfulness than latent code optimization methods such as A&E (Chefer et al. 2023) and D&B (Li et al. 2023) on all prompt-image alignment metrics on the Color-Obj-Scene, COCO-Subject, and COCO-Attribute datasets with complex and challenging prompts, while remaining on par with these methods on simple datasets with prompts created from templates. Moreover, our generated images have better authenticity with more realistic appearances as confirmed by the CLIP-IQA-Real metric and visual comparisons. Although D&B can achieve on-par or higher performance in image quality reflected by CLIP-IQA and HPSv2 metrics on some datasets, it consistently has significantly lower performance than FRAP in CLIP-IQA-Real metric, which shows that our method generates images with better authenticity and a more realistic appearance. Meanwhile, FRAP has lower average latency and lower number of UNet calls than these methods as we do not rely on costly refinement loops which repeatedly call UNet at each time-step, especially on datasets with more complex prompts, e.g., on average 4 seconds faster than D&B for generating one image on the COCO-Subject dataset.

References

- Chang, H.; Zhang, H.; Barber, J.; Maschinot, A.; Lezama, J.; Jiang, L.; Yang, M.-H.; Murphy, K.; Freeman, W. T.; Rubinstein, M.; et al. 2023. Muse: Text-to-image generation via masked generative transformers. *arXiv preprint arXiv:2301.00704*.
- Chefer, H.; Alaluf, Y.; Vinker, Y.; Wolf, L.; and Cohen-Or, D. 2023. Attend-and-excite: Attention-based semantic guidance for text-to-image diffusion models. *ACM Transactions on Graphics (TOG)*, 42(4): 1–10.
- Dhariwal, P.; and Nichol, A. Q. 2021. Diffusion Models Beat GANs on Image Synthesis. In Ranzato, M.; Beygelzimer, A.; Dauphin, Y. N.; Liang, P.; and Vaughan, J. W., eds., *Advances in Neural Information Processing Systems 34: Annual Conference on Neural Information Processing Systems 2021, NeurIPS 2021, December 6-14, 2021, virtual*, 8780–8794.
- Face, H. 2023a. Prompt Weighting. <https://huggingface.co/docs/diffusers/using-diffusers/weighted-prompts>.
- Face, H. 2023b. Stable Diffusion version 1.5. <https://huggingface.co/runwayml/stable-diffusion-v1-5>.
- Feng, W.; He, X.; Fu, T.-J.; Jampani, V.; Akula, A.; Narayana, P.; Basu, S.; Wang, X. E.; and Wang, W. Y. 2022. Training-free structured diffusion guidance for compositional text-to-image synthesis. *arXiv preprint arXiv:2212.05032*.
- Hao, Y.; Chi, Z.; Dong, L.; and Wei, F. 2023. Optimizing Prompts for Text-to-Image Generation. In Oh, A.; Naumann, T.; Globerson, A.; Saenko, K.; Hardt, M.; and Levine, S., eds., *Advances in Neural Information Processing Systems*, volume 36, 66923–66939. Curran Associates, Inc.
- Hertz, A.; Mokady, R.; Tenenbaum, J.; Aberman, K.; Pritch, Y.; and Cohen-Or, D. 2022. Prompt-to-prompt image editing with cross attention control. *arXiv preprint arXiv:2208.01626*.
- Ho, J.; Jain, A.; and Abbeel, P. 2020. Denoising diffusion probabilistic models. *Advances in neural information processing systems*, 33: 6840–6851.
- Ho, J.; and Salimans, T. 2022. Classifier-free diffusion guidance. *arXiv preprint arXiv:2207.12598*.
- Honnibal, M.; and Montani, I. 2017. spaCy 2: Natural language understanding with Bloom embeddings, convolutional neural networks and incremental parsing. To appear.
- Hu, Y.; Liu, B.; Kasai, J.; Wang, Y.; Ostendorf, M.; Krishna, R.; and Smith, N. A. 2023. Tifa: Accurate and interpretable text-to-image faithfulness evaluation with question answering. *arXiv preprint arXiv:2303.11897*.
- Kang, M.; Zhu, J.-Y.; Zhang, R.; Park, J.; Shechtman, E.; Paris, S.; and Park, T. 2023. Scaling up gans for text-to-image synthesis. In *Proceedings of the IEEE/CVF Conference on Computer Vision and Pattern Recognition*, 10124–10134.
- Kingma, D. P.; and Welling, M. 2013. Auto-encoding variational bayes. *arXiv preprint arXiv:1312.6114*.
- Li, J.; Li, D.; Xiong, C.; and Hoi, S. 2022. BLIP: Bootstrapping language-image pre-training for unified vision-language understanding and generation. In *International Conference on Machine Learning*, 12888–12900. PMLR.
- Li, Y.; Keuper, M.; Zhang, D.; and Khoreva, A. 2023. Divide & bind your attention for improved generative semantic nursing. *arXiv preprint arXiv:2307.10864*.
- Lin, T.-Y.; Maire, M.; Belongie, S.; Hays, J.; Perona, P.; Ramanan, D.; Dollár, P.; and Zitnick, C. L. 2014. Microsoft coco: Common objects in context. In *Computer Vision—ECCV 2014: 13th European Conference, Zurich, Switzerland, September 6-12, 2014, Proceedings, Part V 13*, 740–755. Springer.
- Liu, L.; Ren, Y.; Lin, Z.; and Zhao, Z. 2022. Pseudo numerical methods for diffusion models on manifolds. *arXiv preprint arXiv:2202.09778*.
- Liu, V.; and Chilton, L. B. 2022. Design Guidelines for Prompt Engineering Text-to-Image Generative Models. In Barbosa, S. D. J.; Lampe, C.; Appert, C.; Shamma, D. A.; Drucker, S. M.; Williamson, J. R.; and Yatani, K., eds., *CHI '22: CHI Conference on Human Factors in Computing Systems, New Orleans, LA, USA, 29 April 2022 - 5 May 2022*, 384:1–384:23. ACM.
- Marcus, G.; Davis, E.; and Aaronson, S. 2022. A very preliminary analysis of DALL-E 2. *arXiv preprint arXiv:2204.13807*.
- Mañas, O.; Astolfi, P.; Hall, M.; Ross, C.; Urbanek, J.; Williams, A.; Agrawal, A.; Romero-Soriano, A.; and Drozdal, M. 2024. Improving Text-to-Image Consistency via Automatic Prompt Optimization. *arXiv:2403.17804*.
- Midjourney.com. 2023. Midjourney. <https://www.midjourney.com/>.
- Paiss, R.; Chefer, H.; and Wolf, L. 2022. No token left behind: Explainability-aided image classification and generation. In *European Conference on Computer Vision*, 334–350. Springer.
- Podell, D.; English, Z.; Lacey, K.; Blattmann, A.; Dockhorn, T.; Müller, J.; Penna, J.; and Rombach, R. 2023. Sdxl: Improving latent diffusion models for high-resolution image synthesis. *arXiv preprint arXiv:2307.01952*.
- Radford, A.; Kim, J. W.; Hallacy, C.; Ramesh, A.; Goh, G.; Agarwal, S.; Sastry, G.; Askell, A.; Mishkin, P.; Clark, J.; et al. 2021. Learning transferable visual models from natural language supervision. In *International conference on machine learning*, 8748–8763. PMLR.
- Ramesh, A.; Dhariwal, P.; Nichol, A.; Chu, C.; and Chen, M. 2022. Hierarchical text-conditional image generation with clip latents. *arXiv preprint arXiv:2204.06125*, 1(2): 3.
- Rassin, R.; Hirsch, E.; Glickman, D.; Ravfogel, S.; Goldberg, Y.; and Chechik, G. 2023. Linguistic Binding in Diffusion Models: Enhancing Attribute Correspondence through Attention Map Alignment. *arXiv preprint arXiv:2306.08877*.
- Rezende, D. J.; Mohamed, S.; and Wierstra, D. 2014. Stochastic backpropagation and approximate inference in deep generative models. In *International conference on machine learning*, 1278–1286. PMLR.

Rombach, R.; Blattmann, A.; Lorenz, D.; Esser, P.; and Ommer, B. 2022. High-resolution image synthesis with latent diffusion models. In *Proceedings of the IEEE/CVF conference on computer vision and pattern recognition*, 10684–10695.

Ronneberger, O.; Fischer, P.; and Brox, T. 2015. U-net: Convolutional networks for biomedical image segmentation. In *Medical Image Computing and Computer-Assisted Intervention–MICCAI 2015: 18th International Conference, Munich, Germany, October 5-9, 2015, Proceedings, Part III 18*, 234–241. Springer.

Saharia, C.; Chan, W.; Saxena, S.; Li, L.; Whang, J.; Denton, E. L.; Ghasemipour, K.; Gontijo Lopes, R.; Karagol Ayan, B.; Salimans, T.; et al. 2022. Photorealistic text-to-image diffusion models with deep language understanding. *Advances in Neural Information Processing Systems*, 35: 36479–36494.

Sohl-Dickstein, J.; Weiss, E. A.; Maheswaranathan, N.; and Ganguli, S. 2015. Deep Unsupervised Learning using Nonequilibrium Thermodynamics. *Proceedings of the 32nd International Conference on Machine Learning, ICML 2015, Lille, France, 6-11 July 2015*, 37: 2256–2265.

Song, J.; Meng, C.; and Ermon, S. 2020. Denoising diffusion implicit models. *arXiv preprint arXiv:2010.02502*.

Stewart, D. 2023. Damian0815/compel: A prompting Enhancement Library for transformers-type text embedding systems. <https://github.com/damian0815/compel>.

Valerio, R.; Bordalo, J.; Yarom, M.; Bitton, Y.; Szpektor, I.; and Magalhaes, J. 2023. Transferring Visual Attributes from Natural Language to Verified Image Generation. *arXiv preprint arXiv:2305.15026*.

Wang, J.; Chan, K. C.; and Loy, C. C. 2023. Exploring CLIP for Assessing the Look and Feel of Images. In *AAAI*.

Wang, Z. J.; Montoya, E.; Munechika, D.; Yang, H.; Hoover, B.; and Chau, D. H. 2022. Diffusiondb: A large-scale prompt gallery dataset for text-to-image generative models. *arXiv preprint arXiv:2210.14896*.

Witteveen, S.; and Andrews, M. 2022. Investigating Prompt Engineering in Diffusion Models. *arXiv*, abs/2211.15462.

Wu, X.; Hao, Y.; Sun, K.; Chen, Y.; Zhu, F.; Zhao, R.; and Li, H. 2023. Human Preference Score v2: A Solid Benchmark for Evaluating Human Preferences of Text-to-Image Synthesis. *arXiv preprint arXiv:2306.09341*.

Supplementary Material

This supplementary material to our main paper has the following sections:

- In Section “Implementation and Evaluation Details”, we provide the algorithm overview, implementation details, and evaluation settings.
- In Section “Detailed Results”, we present more details of our quantitative results and additional qualitative (visual) comparison examples. In addition, we provided the result for the human evaluations of FRAP and other methods.
- In Section “Ablation Study”, we present an ablation study on the design of FRAP.
- In Section “Additional Quantitative Evaluations”, we present additional quantitative evaluations on additional baseline methods, additional large evaluation datasets, and applying FRAP to the SDXL model.

Implementation and Evaluation Details

Algorithm Overview

In Algorithm 1, we provide the detailed algorithm of our proposed FRAP method.

Algorithm 1: Algorithm Overview of FRAP

Input: Conditional text embedding c^y , unconditional text embedding c^\emptyset , trained *SD* model, decoder \mathcal{D}

Output: The generated image \mathcal{I}

Selection of Latent Code:

- 1: $z_T^b \sim \mathcal{N}(0, 1), \forall b \in \{1, 2, \dots, B\}$
- 2: $Z_T \leftarrow [z_T^1, z_T^2, \dots, z_T^B]$ \triangleright Batch of Initial Latents
- 3: **for** $t = T, T-1, \dots, t_{\text{select}}$ **do**
- 4: $Z_{t-1}, [A_t^1, A_t^2, \dots, A_t^B] \leftarrow SD(Z_t, t, c^y, c^\emptyset)$
- 5: **end for**
- 6: $b^* \leftarrow \operatorname{argmin}_{b \in \{1, 2, \dots, B\}} \mathcal{L}(A_{t_{\text{select}}}^b)$

Adaptive Prompt Weighting:

- 1: $z_T \leftarrow z_T^{b^*}, \alpha_T \leftarrow \vec{0}$
 - 2: **for** $t = T, T-1, \dots, t_{\text{end}}$ **do** \triangleright Adaptive Prompt Weighting
 - 3: $\phi_t \leftarrow \phi_{LB} + (\phi_{UB} - \phi_{LB})\sigma(\alpha_t)$
 - 4: $\tilde{c}^y \leftarrow \phi_t \odot c^y + (1 - \phi_t) \odot c^\emptyset$
 - 5: $z_{t-1}, A_t \leftarrow SD(z_t, t, \tilde{c}^y, c^\emptyset)$
 - 6: $\alpha_{t-1} \leftarrow \alpha_t - \eta_t \cdot \nabla_{\alpha_t} \mathcal{L}(A_t)$
 - 7: **end for**
 - 8: **for** $t = t_{\text{end}} - 1, \dots, 1$ **do** \triangleright No Prompt Weighting
 - 9: $z_{t-1} \leftarrow SD(z_t, t, c^y, c^\emptyset)$
 - 10: **end for**
 - 11: **Return** $\mathcal{I} \leftarrow \mathcal{D}(z_0)$
-

Implementation Details

Following (Chefer et al. 2023; Li et al. 2023), we use the 16×16 CA units for computing the objective function. The weight of object-modifier binding loss $\lambda = 1$. For the optimization in Eq. (9), we use a constant step-size $\eta_t = \eta = 1$. Chefer et al. (2023) observed that the final time-steps do not alter the spatial locations/structures of objects. As a result,

we apply our adaptive prompt weighting method to a subset of time-steps $t = T, T-1, \dots, t_{\text{end}}$, where $T = 50$ and $t_{\text{end}} = 26$.⁷

For our adaptive prompt weighting method, the token weighting coefficients ϕ for the special $\langle \text{spot} \rangle$, $\langle \text{eot} \rangle$ and $\langle \text{padding} \rangle$ tokens are set to 1 and are frozen (i.e., not updated). Similar to the suggested prompt weighting values of (Hertz et al. 2022), we set the lower and upper bound of per-token weighting coefficients to $\phi \in [\phi_{LB} = 0.6, \phi_{UB} = 1.4]$. For selecting the initial latent code, we perform 15 steps of inference from $t = T = 50$ to $t_{\text{select}} = 36$ with a batch of $|B| = 4$ noisy latent codes sampled from $\mathcal{N}(0, 1)$. Following the other hyperparameters used by Chefer et al. (2023), we use CFG guidance scale $\beta = 7.5$ and the Gaussian filter kernel size is 3 with a standard deviation of 0.5.

Experimental Settings

Baselines. We compare our approach with three baseline methods. (i) Stable Diffusion (SD) (Rombach et al. 2022), (ii) Attend-and-Excite (A&E) (Chefer et al. 2023), and (iii) Divide&Bind (D&B) (Li et al. 2023). For the A&E (Chefer et al. 2023) and D&B (Li et al. 2023) baselines, we follow their default settings in the papers and implementations. All baselines and our approach are evaluated based on the Stable Diffusion 1.5 (Rombach et al. 2022; Face 2023b) model following the choice of D&B (Li et al. 2023) at FP16 precision with its default PNDM (Liu et al. 2022) scheduler. Our additional experiments show that FRAP is also applicable to SDXL (Podell et al. 2023) and can also improve its performance (see Table 12).

Object and Modifier Identification. In order to automate the manual identification of object tokens and modifier tokens, we used the spaCy’s transformer-based dependency parser (Honnibal and Montani 2017) (also used by Syn-Gen (Chefer et al. 2023)) to automatically extract a set of object noun tokens S and a set of modifier tokens R . To guarantee the correctness of automatically extracted noun and modifiers, human can manually check the predictions and make any correction if necessary.

Datasets. The recent methods A&E (Chefer et al. 2023) and D&B (Li et al. 2023) introduce new prompt datasets for evaluating the effectiveness of a T2I model in handling catastrophic neglect and modifier binding. In this work, we adopt the same datasets (summarized in Table 3) and use them for the evaluation of all the baselines. For all dataset used in the experiments of the main paper, we generate 64 images for each prompt using the same set of 64 seeds for each evaluated method.

A&E (Chefer et al. 2023) introduce three *simple* evaluation datasets:

⁷Note that we are overloading the term “time-step” here. What we mean by *time-step*, going forward, is the *jump index*. That is, going from $T = 50$ to $T = 49$, for example, we are in fact jumping from actual time-step 1000 to $1000 - \frac{1000}{50} = 980$. We could decide to perform inference in fewer [or more] number of jumps, however, we use the default value of 50 to remain comparable to the literature.

1. **Animal-Animal**, which handles the simple cases with two animal objects in the prompt (evaluates the *catatrophic neglect* issue).
2. **Color-Object**, which assigns a color to each of the two objects (evaluates the *modifier binding* issue).
3. **Animal-Object**, which has prompts with an animal and a colored object.
D&B (Li et al. 2023) introduce five more *complex* evaluation datasets with higher prompt complexity:
 4. **Animal-Scene**, which contains a scene or scenario in the prompt, along with two animal tokens.
 5. **Color-Object-Scene**, which introduces a scene or scenario along with the two colored objects.
 6. **Multi-Object**, which aims to present multiple object entities in the prompt with a count.
 7. **COCO-Subject**, which focuses on the objects-related prompts filtered from MSCOCO (Lin et al. 2014) captions used in (Hu et al. 2023) with up to four objects and without modifiers.
 8. **COCO-Attribute**, which focuses on the modifier-related prompts filtered from MSCOCO (Lin et al. 2014) captions used in (Hu et al. 2023) with up to two objects and with diverse modifiers.

Table 3: Description of datasets used in our experiments.

Dataset (# Prompts)	Description
Animal-Animal (66) (Chefer et al. 2023)	a [animalA] and a [animalB]
Color-Object (66) (Chefer et al. 2023)	a [colorA][subjectA] and a [colorB][subjectB]
Animal-Object (144) (Chefer et al. 2023)	a [animal] and a [color][object]
Animal-Scene (56) (Li et al. 2023)	a [animalA] and a [animalB] [scene]
Color-Obj-Scene (60) (Li et al. 2023)	a [colorA][subjectA] and a [colorB][subjectB][scene]
Multi-Object (30) (Li et al. 2023)	more than two objects or instances in the image
COCO-Subject (30) (Li et al. 2023)	filtered COCO captions related to subjects in the image
COCO-Attribute (27) (Li et al. 2023)	filtered COCO captions related to the attributes

Evaluation Metrics. To quantitatively evaluate the prompt-image alignment of our proposed approach, we use the metrics adopted by both A&E (Chefer et al. 2023) and D&B (Li et al. 2023). To evaluate the image quality of images generated with our approach, we additionally use Image Quality Assessment (IQA) metrics (Wu et al. 2023; Wang, Chan, and Loy 2023).

To evaluate the prompt-image alignment, we consider the following metrics in our experimental evaluation:

- **Full-prompt Similarity (Full-CLIP) (Chefer et al. 2023).** This metric computes the average cosine CLIP similarity between the prompt text embedding and generated image embedding.

- **Minimum Object Similarity (MOS) (Chefer et al. 2023).** Paiss *et al.* (Paiss, Chefer, and Wolf 2022) observed that only using the Full-CLIP to estimate the prompt-image alignment may not be completely reliable, as a high Full-CLIP score is still achievable even when a few objects are missing in the generated image. MOS measures the minimum cosine similarity between the image embedding and text embeddings of each sub-prompt containing an object mentioned in the prompt.
- **Text-to-Text Similarity (TTS) (Chefer et al. 2023; Li et al. 2023).** TTS computes the cosine similarity between the embeddings of (i) original text prompt and (ii) caption of the synthesized image generated with a captioning model such as BLIP (Li et al. 2022).

To evaluate the generated image quality, we consider the following Image Quality Assessment (IQA) metrics in our experimental evaluation:

- **Human Preference Score v2 (HPSv2) (Wu et al. 2023).** HPSv2 metric reflects the human preference so it evaluates the image authenticity, quality, and faithfulness to the prompt. It is a scoring mechanism which is built on top of CLIP, by fine-tuning on Human-Preference Dataset v2 (HPDv2) (Wu et al. 2023) to accurately predict the human preferences for synthesized images.
- **CLIP-IQA (Wang, Chan, and Loy 2023).** This metric assesses both the quality perception (i.e., the general look of the images: e.g., overall quality, brightness, etc.) and abstract perception (i.e., the general feel of the image: e.g., aesthetic, happy, etc.). Specifically, we consider the averaged CLIP-IQA score on four aspects including (“quality”, “noisiness”, “natural”, and “real”) to evaluate the overall image quality of the generated image. In addition, we use the CLIP-IQA-Real score on the “real” aspect to evaluate the level of image authenticity.

Latency. Our reported latency measures the average wall-clock time for generating one image on each dataset in seconds with a V100 GPU.

Detailed Results

Detailed Quantitative Results. For the experiments in the main paper, we present the detailed results on all eight datasets in Table 4.

We observe in Table 4 that, on datasets with *simple* handcrafted templates (S-AA, S-CO, and S-AO), there is a tight competition among A&E, D&B, and FRAP across all metrics, while all three exceed the performance of SD. This basically shows that the *simple* datasets may not be sufficient to definitively identify the superior method among the competing options.

We see a clear advantage of FRAP on more challenging *complex* datasets. In Table 4, we observe that FRAP consistently outperforms all other methods in almost all metrics on the *complex* datasets. Specifically, FRAP is consistently best on *complex* datasets in terms of TTS, Full-CLIP, HPSv2, and CLIP-IQA-Real metrics, which demonstrates the ability of FRAP to generate realistic images in various complicated scenarios. FRAP surpasses its competitors in all evalu-

ation metrics on the C-CS and C-CA datasets, which contain more realistic real-world prompts compared to the manually crafted datasets.

We observe in Table 4 that FRAP performs well on most evaluation datasets, except for the Multi-Object dataset, where all methods struggle to generate the correct number of dogs and cats (e.g., see the bottom-right of Fig. 5). In general, delivering a correct count of objects in generated images is still an open challenge.

Additional Qualitative Results. In Figs. 5, 6 and 7, we provide additional visual comparisons among FRAP and other methods on prompts from eight different datasets. As shown in the figures, FRAP generates images that are more faithful to the prompt containing all the mentioned objects without hybrid objects and have accurate modifier bindings. Moreover, images generated with FRAP maintain a more realistic appearance.

In Fig. 8, we provide visual comparisons of FRAP, the LLM prompt rewrite method Promptist (Hao et al. 2023), and the result of combining FRAP and Promptist. The quantitative results are provided in Table. 2 of the main paper.

Human Evaluations. In addition to quantitative evaluation metrics, we perform human evaluations by randomly selecting 60 prompts from the 4 complex datasets (i.e. C-COS, C-CS, C-CA, and C-AS datasets). For each prompt, we ask 6 participants to choose the best image among the outputs of SD, A&E, D&B, and FRAP. When presenting each prompt, we randomly shuffle the order of the images from different methods to ensure an unbiased evaluation. FRAP is voted as the majority winner in 42.1% of the test-cases and significantly outperformed others (i.e. SD with 10.5%, A&E with 22.8%, and D&B with 24.6%), which also aligns with our quantitative findings using the automated evaluation metrics. We demonstrate the interface of the human evaluation in Fig. 9.

Ablation Study

In this section, we present ablation studies for different design aspects of FRAP. For all ablation experiments, we generate 16 images for each prompt using the same set of 16 seeds for each evaluated variant of FRAP. We report the same prompt-image alignment metrics and image quality assessment metrics used in the main paper and provide details on the metrics in the “Experimental Settings” subsection.

Objective Function. First, we ablate the design of our unified objective function \mathcal{L} . In Table 5, we remove the binding loss $\mathcal{L}_{\text{binding}}$ in the second row and remove the presence loss $\mathcal{L}_{\text{presence}}$ in the third row. We observe that removing the binding loss has a smaller impact while removing the presence has a significant drop in performance. It shows the important role of object presence loss in improving both prompt-image alignment and image quality since the presence of each object is fundamental to the faithfulness of the image. Overall, using both loss terms achieves the highest performance. Therefore, we use both loss terms for our approach by default.

Furthermore, to better understand the internal workings of the method, we visualize the cross-attention (CA) maps while using only the presence loss, only the binding loss, or both loss terms. In Fig. 3, with only $\mathcal{L}_{\text{presence}}$, objects are separated but color green leaks to the crown. With only $\mathcal{L}_{\text{binding}}$, the color binding is correct but two objects are overlapped. Overall, using both loss components achieves the best result.

In the fourth row of Table 5, we attempt to use only the loss from the most neglected token with the lowest max activation. This max variant, similar to the loss in A&E (Chefer et al. 2023), results in lower performance than our default approach. The higher performance shows the advantage of our presence loss design which uses the *mean* among all objects as the total object presence loss and enhances the presence of all objects instead of a single one, which is essential for complex prompts with multiple objects.

In Table 6, we ablate the choice of our object presence loss. We replace the object presence loss with the Total Variation loss (Li et al. 2023). Our proposed object presence loss in Eq. (5) performs better than the TV loss.

In Table 7, we compare our object-modifier binding loss to other alternatives. Our proposed object-modifier binding loss in Eq. (6) improves the performance over the JSD (Li et al. 2023) and KLD (Rassin et al. 2023) loss. Our approach of considering the minimum probability essentially filters out the outliers, since the outliers in two distributions rarely overlap, minimizing their impact on our objective. This is unlike KLD and JSD which consider the entire distributions and therefore, can be disproportionately inflated by outliers.

Adaptive Prompt Weighting. In addition, we study the effect of adaptive prompt weighting (APW) and the selection of initial latent code. As shown in Table 8, removing either one will result in lower performance in the prompt-image alignment metrics. Although removing adaptive prompt weighting results in a higher score in the CLIP-IQA metric, the prompt-image alignment performance drops significantly. Overall, using our adaptive prompt weighting method along the initial latent code selection process results in the overall best performance. For qualitative examples of this ablation, see Fig. 4. Without selecting a decent initial latent code, the 1st row images have an “incorrect layout”, e.g. “dog”, “shoe”, and “red” take the majority of the space and the other objects are neglected. In the 2nd row, using the selection alone can find a “good layout” to generate both objects, but the prompt-image alignment is suboptimal in image details compared to the 3rd row using both components (see improved details in dog’s eye and the car).

Also in the last two rows of Table 8, we compare to two manual/static prompt weighting variants, i.e. static prompt weighting with or without initial latent code selection. In both static prompt weighting variants, we set the prompt token weighting coefficients to a fixed value of 1.4 for the object and attribute tokens in the first 25 steps. The results in Table 8 show that both static prompt weighting variants have significantly lower image quality and lower image authenticity reflected by CLIP-IQA and CLIP-IQA-Real metrics. This reflects that our adaptive prompt weighting can preserve the image quality by adaptively setting the weight-

Table 4: Quantitative comparison of FRAP and other methods across 8 different datasets. Higher is better (except for latency). Our reported latency measures the average wall-clock time for generating one image on each dataset in seconds with a V100 GPU. For the experiments in this table, we generate 64 images for each prompt using the same set of 64 seeds for each method.

Dataset	Method	Prompt-Image Alignment			Image Quality Assessment			Latency (s) ↓
		TTS ↑	Full-CLIP ↑	MOS ↑	HPS v2 ↑	CLIP-IQA ↑	CLIP-IQA Real ↑	
Animal-Animal (Chefer et al. 2023)	SD (Rombach et al. 2022)	0.763	0.312	0.217	0.268	0.822	0.937	8.1
	A&E (Chefer et al. 2023)	0.810	0.334	0.250	0.272	0.822	0.937	12.1
	D&B (Li et al. 2023)	0.802	0.330	0.242	0.273	0.836	0.952	12.9
	FRAP (ours)	0.804	0.333	0.245	0.272	0.817	0.962	13.1
Color-Object (Chefer et al. 2023)	SD (Rombach et al. 2022)	0.761	0.338	0.236	0.281	0.617	0.482	7.9
	A&E (Chefer et al. 2023)	0.811	0.363	0.270	0.286	0.617	0.482	12.1
	D&B (Li et al. 2023)	0.804	0.357	0.261	0.286	0.637	0.519	14.9
	FRAP (ours)	0.802	0.357	0.259	0.286	0.653	0.566	13.6
Animal-Object (Chefer et al. 2023)	SD (Rombach et al. 2022)	0.791	0.343	0.247	0.277	0.756	0.826	7.8
	A&E (Chefer et al. 2023)	0.833	0.357	0.267	0.283	0.755	0.824	11.6
	D&B (Li et al. 2023)	0.831	0.351	0.261	0.284	0.770	0.817	12.5
	FRAP (ours)	0.835	0.361	0.267	0.283	0.763	0.874	13.2
Animal-Scene (Li et al. 2023)	SD (Rombach et al. 2022)	0.736	0.347	0.229	0.273	0.777	0.928	8.0
	A&E (Chefer et al. 2023)	0.741	0.354	0.243	0.275	0.777	0.928	17.3
	D&B (Li et al. 2023)	0.755	0.356	0.239	0.276	0.789	0.963	16.8
	FRAP (ours)	0.758	0.360	0.236	0.276	0.779	0.964	13.8
Color-Obj-Scene (Li et al. 2023)	SD (Rombach et al. 2022)	0.707	0.366	0.254	0.282	0.675	0.770	8.0
	A&E (Chefer et al. 2023)	0.708	0.376	0.267	0.286	0.675	0.770	17.9
	D&B (Li et al. 2023)	0.719	0.375	0.264	0.286	0.682	0.808	16.7
	FRAP (ours)	0.727	0.381	0.269	0.287	0.676	0.835	14.3
Multi-Object (Li et al. 2023)	SD (Rombach et al. 2022)	0.763	0.304	0.244	0.264	0.792	0.811	8.0
	A&E (Chefer et al. 2023)	0.793	0.315	0.263	0.266	0.792	0.811	12.3
	D&B (Li et al. 2023)	0.789	0.314	0.258	0.270	0.816	0.824	13.7
	FRAP (ours)	0.783	0.311	0.256	0.266	0.804	0.869	13.2
COCO-Subject (Li et al. 2023)	SD (Rombach et al. 2022)	0.829	0.331	0.250	0.278	0.805	0.852	7.9
	A&E (Chefer et al. 2023)	0.829	0.333	0.254	0.277	0.805	0.852	19.1
	D&B (Li et al. 2023)	0.835	0.333	0.253	0.279	0.814	0.862	18.1
	FRAP (ours)	0.837	0.334	0.255	0.279	0.814	0.866	14.0
COCO-Attribute (Li et al. 2023)	SD (Rombach et al. 2022)	0.817	0.347	0.245	0.286	0.703	0.750	8.1
	A&E (Chefer et al. 2023)	0.820	0.353	0.254	0.286	0.703	0.750	15.3
	D&B (Li et al. 2023)	0.821	0.353	0.251	0.288	0.720	0.760	16.7
	FRAP (ours)	0.838	0.358	0.254	0.289	0.725	0.778	13.9

ing coefficients, while the manual prompt weighting results in degraded image quality due to using a constant value throughout the generation and requiring humans to select its values manually.

For the Redo Time-step variant in Table 9, after updating α based on Eq. (10), we use the updated α to redo the current time-step t instead of using it in the next time-step $t - 1$. From the results, we observe that our default setting of using the updated α in the next time-step $t - 1$ achieves higher performance in IQA metrics while having lower latency. The lower latency is due to only performing one UNet call at each time-step instead of two UNet calls which is required when redoing each time-step.

Moreover, we compare different number of time-steps to perform adaptive prompt weighting in Table 9. By default, we use $t_{\text{end}} = 26$ so the adaptive prompt weighting is applied to the first 25 steps in the reverse generative process (RGP). By using adaptive prompt weighting only in the first 10 steps in the RGP with $t_{\text{end}} = 41$, there is a slight drop in prompt-image alignment and a slight increase in IQA metric scores. When using adaptive prompt weighting in all 50

RGP steps with $t_{\text{end}} = 1$, the latency increases with no significant benefit in performance. This aligns with the observation of Chefer *et al.* (Chefer et al. 2023) that the final time-steps do not alter the spatial locations/structures of objects. Therefore, we use $t_{\text{end}} = 26$ to achieve a good balance between performance and latency.

Additional Quantitative Evaluations

Additional Baselines. In Table 10, we compare FRAP with two additional text-to-image methods SynGen (Rassin et al. 2023) and StructureDiffusion (Feng et al. 2022). Although SynGen and StructureDiffusion has competitive CLIP-IQA score with similar latency to SD, these two approaches fall short in the prompt-image alignment scores. Overall, FRAP has consistently higher prompt-image alignment scores and is also competitive in the IQA metrics.

Additional Datasets. In addition to the eight datasets listed in Table 3, we further evaluate FRAP and the other methods on the DrawBench (Saharia et al. 2022) dataset and the ABC-6K (Feng et al. 2022) dataset. For the Draw-

Table 5: Ablation study on the binding loss $\mathcal{L}_{\text{binding}}$, presence loss $\mathcal{L}_{\text{presence}}$, and max aggregation of per-object presence losses $\mathcal{L}_{\text{presence}}^s$. The default setting using both $\mathcal{L}_{\text{binding}}$ and $\mathcal{L}_{\text{presence}}$ achieves the overall best performance in both prompt-image alignment and image quality. We generate 16 images for each prompt in the COCO-Attribute (Li et al. 2023) dataset using the same set of 16 seeds for each evaluated variant of FRAP.

Method	Prompt-Image Alignment			Image Quality Assessment			Latency (s) ↓
	TTS ↑	Full-CLIP ↑	MOS ↑	HPS v2 ↑	CLIP-IQA ↑	CLIP-IQA Real ↑	
FRAP (default)	0.836	0.359	0.256	0.289	0.722	0.773	14.1
w/o $\mathcal{L}_{\text{binding}}$	0.837	0.359	0.255	0.289	0.720	0.772	14.1
w/o $\mathcal{L}_{\text{presence}}$	0.807	0.341	0.239	0.284	0.707	0.756	13.9
max $\mathcal{L}_{\text{presence}}^s$	0.827	0.352	0.252	0.288	0.712	0.752	14.1

Table 6: Comparison of our object presence loss $\mathcal{L}_{\text{presence}}$ and the Total Variation (TV) loss (Li et al. 2023). Our object presence loss $\mathcal{L}_{\text{presence}}$ achieves better performance in both prompt-image alignment and image quality. We generate 16 images for each prompt in the Color-Obj-Scene (Li et al. 2023) dataset using the same set of 16 seeds for each loss.

Method	Prompt-Image Alignment			Image Quality Assessment			Latency (s) ↓
	TTS ↑	Full-CLIP ↑	MOS ↑	HPS v2 ↑	CLIP-IQA ↑	CLIP-IQA Real ↑	
FRAP ($\mathcal{L}_{\text{presence}}$)	0.725	0.380	0.269	0.287	0.670	0.829	13.9
FRAP (TV)	0.718	0.375	0.263	0.286	0.664	0.806	14.0

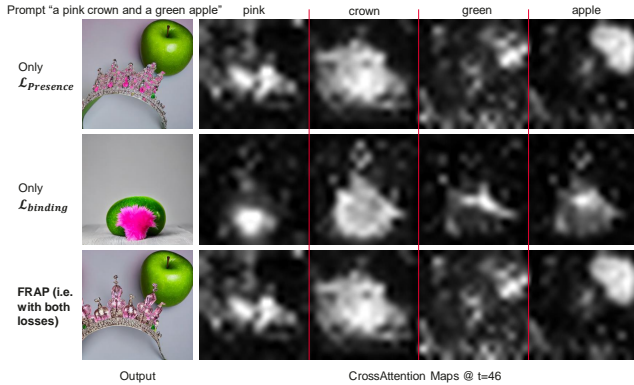


Figure 3: Visualization of cross-attention maps while using different loss function components.

Bench (Saharia et al. 2022) dataset, we use a total of 183 comprehensive prompts excluding 7 prompts from the ‘‘Rare Words’’ category and 10 prompts from the ‘‘Misspellings’’ category since these are not within the scope of this paper or the other considered baselines. The ABC-6K (Feng et al. 2022) dataset contains 6.4K prompts filtered from MSCOCO (Lin et al. 2014) where each contains at least two color words modifying different objects. For the DrawBench dataset, we generate 16 images for each prompt using the same set of 16 seeds for each method. For the ABC-6K dataset, we generate one image for each prompt using the same seed for each method.

As shown in Table 11, FRAP outperforms the other methods in terms of four out of six evaluated metrics while having a lower latency than A&E (Chefer et al. 2023) and D&B (Li et al. 2023) on the DrawBench (Saharia et al. 2022) dataset. Moreover, FRAP significantly outperforms the other methods in all metrics in terms of both prompt-image alignment

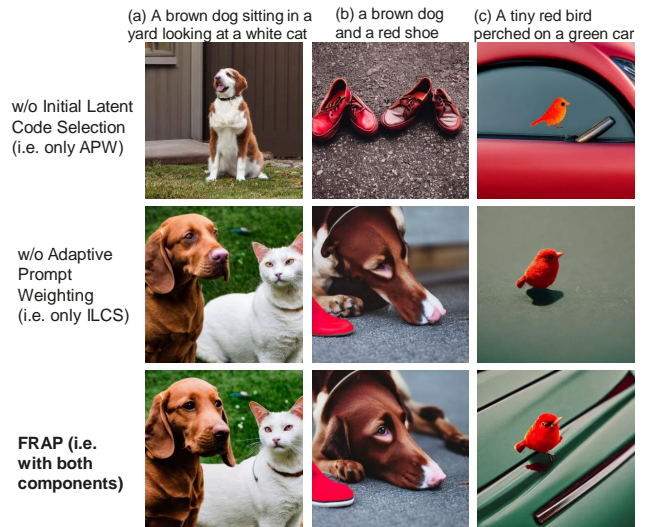


Figure 4: Qualitative examples for the ablation on adaptive prompt weighting and initial latent code selection.

and image quality on the ABC-6K (Feng et al. 2022) dataset.

SDXL model. In addition, we perform additional experiments on the SDXL (Podell et al. 2023) model. We observe the vanilla SDXL also suffers from catastrophic neglect and incorrect modifier binding issues. In Table 12, our results on SDXL show that FRAP is generalizable to different T2I diffusion models and it can enhance the prompt-image alignment and image authenticity of the SDXL model.

Table 7: Comparison of our object-modifier binding loss $\mathcal{L}_{\text{binding}}$ and the JSD loss (Li et al. 2023) and KLD loss (Rassin et al. 2023). Our object-modifier binding loss $\mathcal{L}_{\text{binding}}$ achieves better performance in both prompt-image alignment and image quality. We generate 16 images for each prompt in the Color-Obj-Scene (Li et al. 2023) dataset using the same set of 16 seeds for each loss.

Method	Prompt-Image Alignment			Image Quality Assessment			Latency (s) ↓
	TTS ↑	Full-CLIP ↑	MOS ↑	HPS v2 ↑	CLIP-IQA ↑	CLIP-IQA Real ↑	
FRAP ($\mathcal{L}_{\text{binding}}$)	0.725	0.380	0.269	0.287	0.670	0.829	13.9
FRAP (JSD)	0.721	0.380	0.266	0.286	0.662	0.825	14.1
FRAP (KLD)	0.724	0.380	0.267	0.287	0.668	0.831	14.2

Table 8: Ablation study on adaptive prompt weighting and the selection of initial latent code. The default setting using both adaptive prompt weighting and initial latent code selection achieves the overall best performance in both prompt-image alignment and image quality. We generate 16 images for each prompt in the COCO-Attribute (Li et al. 2023) dataset using the same set of 16 seeds for each evaluated variant of FRAP.

Method	Prompt-Image Alignment			Image Quality Assessment			Latency (s) ↓
	TTS ↑	Full-CLIP ↑	MOS ↑	HPS v2 ↑	CLIP-IQA ↑	CLIP-IQA Real ↑	
FRAP (default)	0.836	0.359	0.256	0.289	0.722	0.773	14.1
w/o Initial Latent Code Selection	0.829	0.354	0.250	0.287	0.718	0.746	10.5
w/o Adaptive Prompt Weighting	0.828	0.354	0.253	0.288	0.723	0.797	13.1
with Static Prompt Weighting	0.841	0.356	0.249	0.288	0.692	0.694	5.2
with Static Prompt Weighting, w/o Initial Latent Code Selection	0.844	0.358	0.250	0.288	0.689	0.697	9.3

Table 9: Ablation study on the number of time-steps to apply adaptive prompt weighting. We generate 16 images for each prompt in the COCO-Attribute (Li et al. 2023) dataset using the same set of 16 seeds for each evaluated variant of FRAP.

Method	Prompt-Image Alignment			Image Quality Assessment			Latency (s) ↓
	TTS ↑	Full-CLIP ↑	MOS ↑	HPS v2 ↑	CLIP-IQA ↑	CLIP-IQA Real ↑	
FRAP (default)	0.836	0.359	0.256	0.289	0.722	0.773	14.1
Redo Time-step	0.840	0.359	0.256	0.289	0.716	0.766	16.1
$t_{\text{end}} = 41$	0.832	0.355	0.254	0.289	0.726	0.787	13.6
$t_{\text{end}} = 1$	0.837	0.360	0.256	0.289	0.718	0.769	15.3

Table 10: Additional quantitative comparison of FRAP with two additional text-to-image methods SynGen (Rassin et al. 2023) and StructureDiffusion (Feng et al. 2022). For the experiments in this table, we generate 16 images for each prompt using the same set of 16 seeds for each method.

Dataset	Method	Prompt-Image Alignment			Image Quality Assessment			Latency (s) ↓
		TTS ↑	Full-CLIP ↑	MOS ↑	HPS v2 ↑	CLIP-IQA ↑	CLIP-IQA Real ↑	
COCO-Subject (Li et al. 2023)	SD (Rombach et al. 2022)	0.829	0.330	0.249	0.278	0.810	0.863	8.2
	SynGen (Rassin et al. 2023)	0.827	0.334	0.255	0.279	0.819	0.863	6.4
	StructureDiffusion (Feng et al. 2022)	0.827	0.331	0.249	0.277	0.811	0.884	6.0
	A&E (Chefer et al. 2023)	0.829	0.333	0.252	0.277	0.801	0.843	19.1
	D&B (Li et al. 2023)	0.835	0.333	0.252	0.279	0.812	0.855	17.7
	FRAP (ours)	0.839	0.335	0.255	0.279	0.812	0.871	13.3
COCO-Attribute (Li et al. 2023)	SD (Rombach et al. 2022)	0.815	0.345	0.245	0.287	0.710	0.746	7.7
	SynGen (Rassin et al. 2023)	0.818	0.352	0.250	0.287	0.736	0.774	7.6
	StructureDiffusion (Feng et al. 2022)	0.822	0.349	0.246	0.285	0.712	0.767	6.0
	A&E (Chefer et al. 2023)	0.813	0.354	0.255	0.286	0.697	0.731	14.9
	D&B (Li et al. 2023)	0.822	0.351	0.250	0.288	0.716	0.750	16.5
	FRAP (ours)	0.836	0.359	0.256	0.289	0.722	0.773	14.1

Table 11: Additional quantitative comparison of FRAP and other methods on two additional datasets DrawBench (Saharia et al. 2022) and ABC-6K (Feng et al. 2022). For the DrawBench dataset, we generate 16 images for each prompt using the same set of 16 seeds for each method. For the ABC-6K dataset, we generate one image for each prompt using the same seed for each method.

Dataset	Method	Prompt-Image Alignment			Image Quality Assesment			Latency (s) ↓
		TTS ↑	Full-CLIP ↑	MOS ↑	HPS v2 ↑	CLIP-IQA ↑	CLIP-IQA Real ↑	
DrawBench (Saharia et al. 2022)	SD (Rombach et al. 2022)	0.713	0.329	0.243	0.275	0.703	0.820	8.1
	A&E (Chefer et al. 2023)	0.718	0.336	0.251	0.275	0.710	0.826	18.8
	D&B (Li et al. 2023)	0.720	0.334	0.248	0.276	0.722	0.832	17.6
	FRAP (ours)	0.722	0.336	0.248	0.277	0.717	0.837	14.5
ABC-6K (Feng et al. 2022)	SD (Rombach et al. 2022)	0.771	0.332	0.249	0.282	0.675	0.698	7.9
	A&E (Chefer et al. 2023)	0.767	0.334	0.251	0.281	0.675	0.697	19.3
	D&B (Li et al. 2023)	0.771	0.333	0.250	0.283	0.688	0.703	18.3
	FRAP (ours)	0.783	0.338	0.253	0.284	0.726	0.788	14.2

Table 12: Additional quantitative results on applying FRAP to the SDXL (Podell et al. 2023) model. For the experiments in this table, we generate 16 images for each prompt using the same set of 16 seeds for each method.

Dataset	Method	Prompt-Image Alignment			Image Quality Assesment			Latency (s) ↓
		TTS ↑	Full-CLIP ↑	MOS ↑	HPS v2 ↑	CLIP-IQA ↑	CLIP-IQA Real ↑	
Color-Obj-Scene (Li et al. 2023)	SDXL (Podell et al. 2023)	0.742	0.388	0.267	0.293	0.791	0.940	27.2
	FRAP (with SDXL)	0.744	0.391	0.272	0.295	0.789	0.943	44.7
Multi-Object (Li et al. 2023)	SDXL (Podell et al. 2023)	0.785	0.307	0.249	0.264	0.838	0.903	28.7
	FRAP (with SDXL)	0.787	0.311	0.253	0.266	0.842	0.901	44.1
COCO-Subject (Li et al. 2023)	SDXL (Podell et al. 2023)	0.844	0.346	0.257	0.283	0.825	0.830	29.0
	FRAP (with SDXL)	0.845	0.347	0.257	0.284	0.832	0.836	45.6

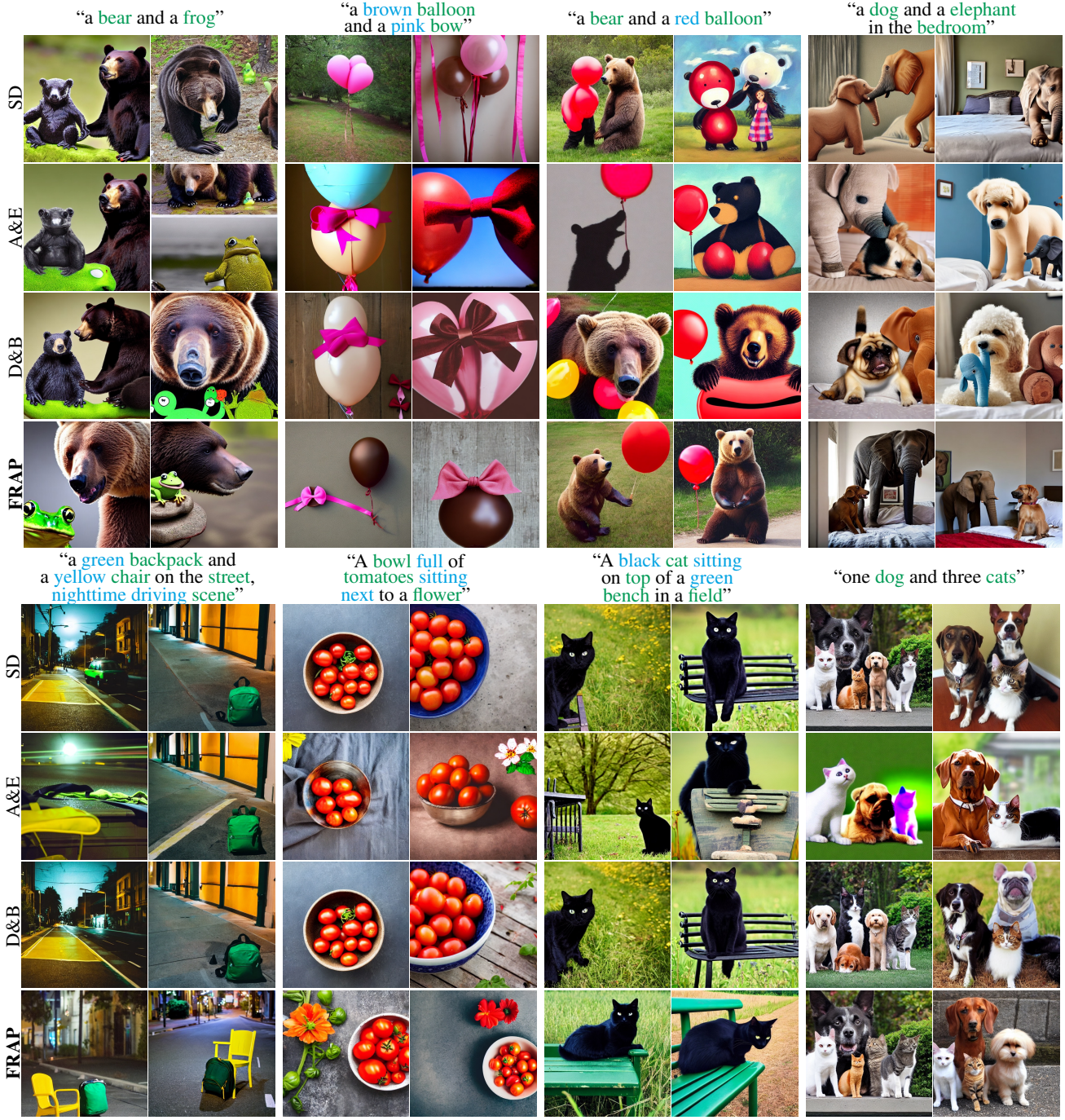


Figure 5: **Qualitative comparison on prompts from all eight datasets.** For each prompt, we show images generated by all four methods (using the same set of seeds). The object tokens are highlighted in green and modifier tokens are highlighted in blue.

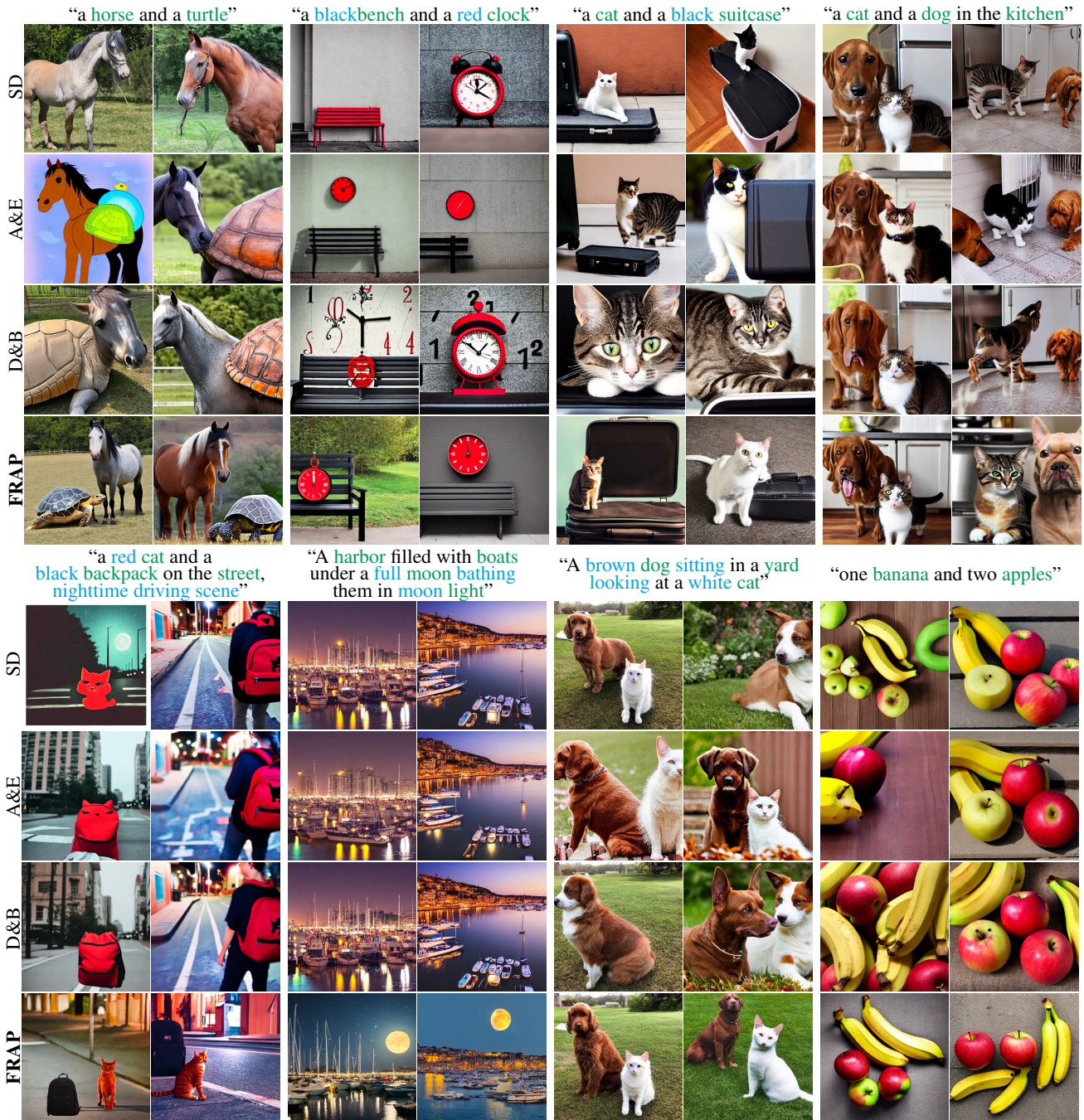


Figure 6: **Qualitative comparison on prompts from all eight datasets.** For each prompt, we show images generated by all four methods, where we use the same set of seeds. The object tokens are highlighted in green and modifier tokens are highlighted in blue.

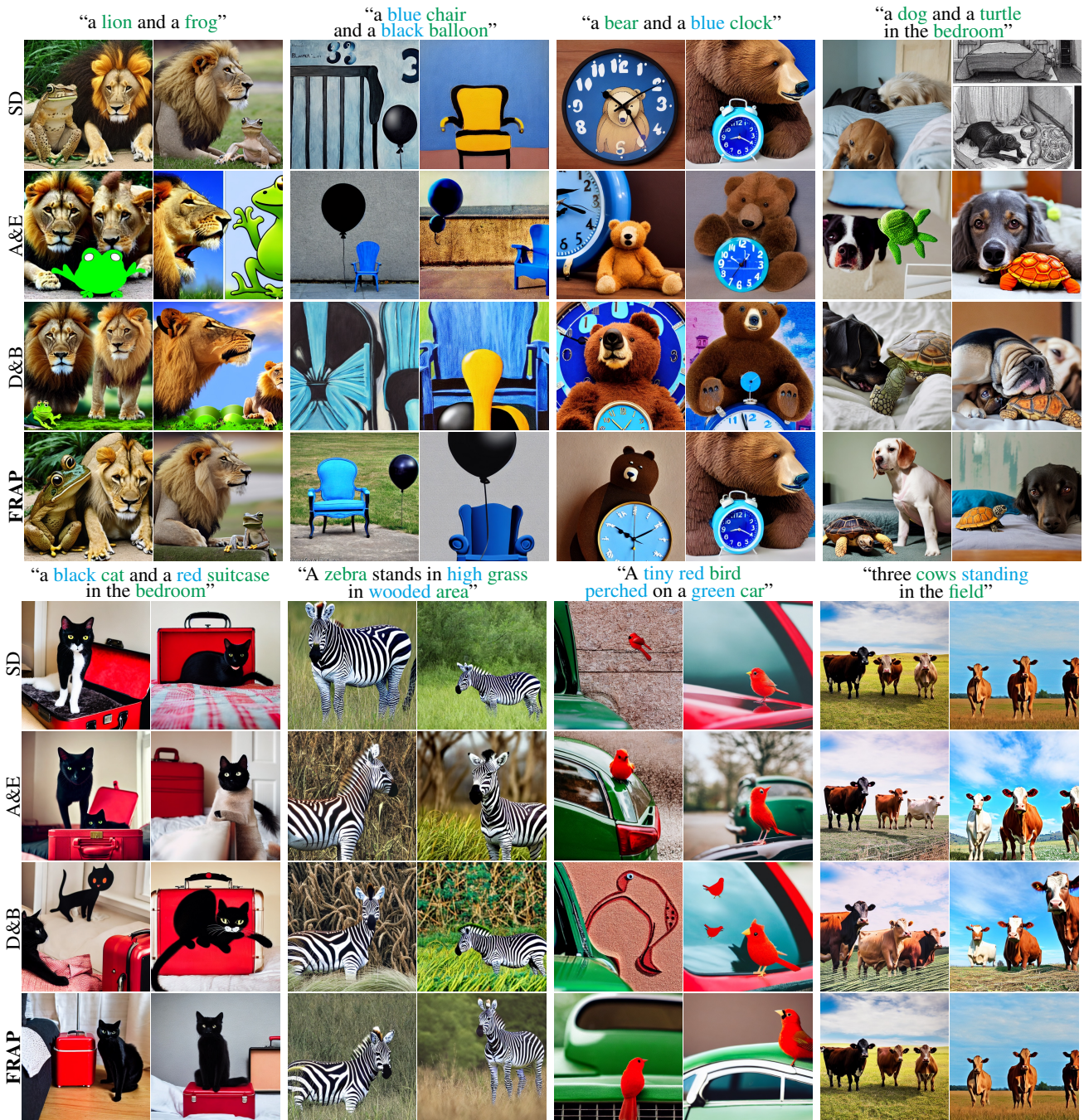


Figure 7: **Qualitative comparison on prompts from all eight datasets.** For each prompt, we show images generated by all four methods, where we use the same set of seeds. The object tokens are highlighted in green and modifier tokens are highlighted in blue.

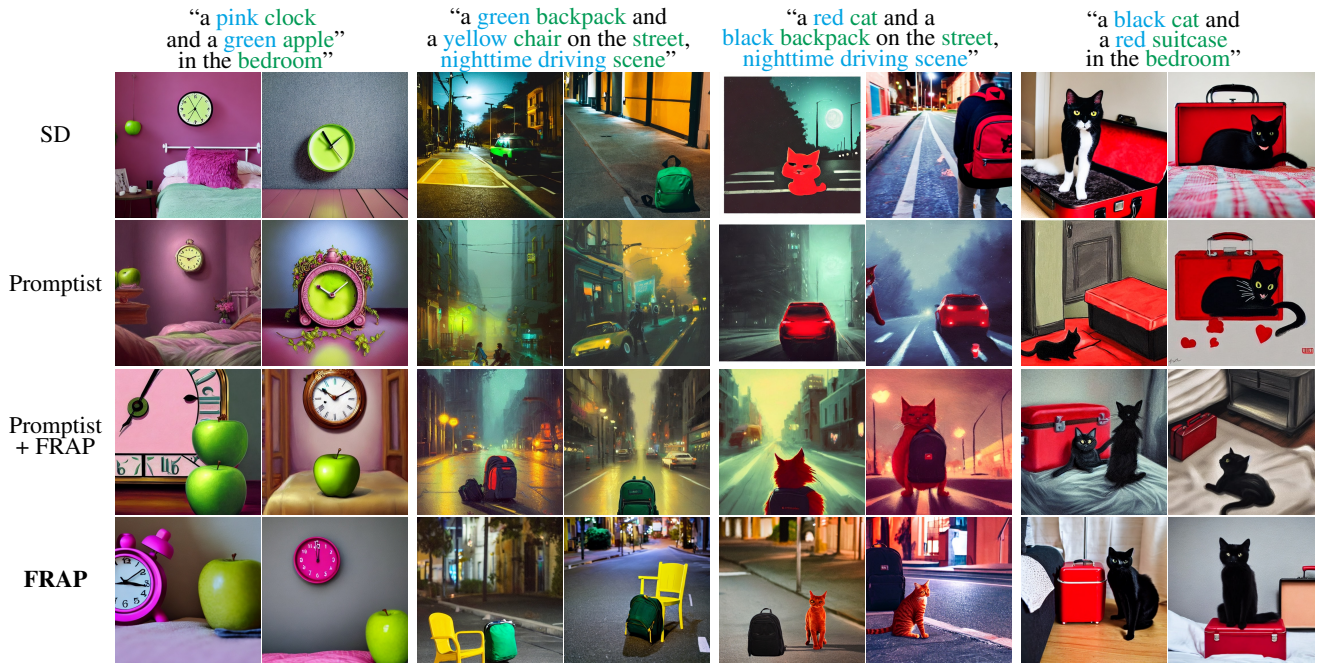


Figure 8: Qualitative comparisons of SD, training-based LLM prompt optimization/rewrite method Promptist (Hao et al. 2023), applying FRAP on Promptist rewritten prompt, and FRAP, on the *complex* Color-Object-Scene dataset. For each prompt, we show images generated by all four methods (using the same set of seeds). The object tokens are highlighted in green and modifier tokens are highlighted in blue.

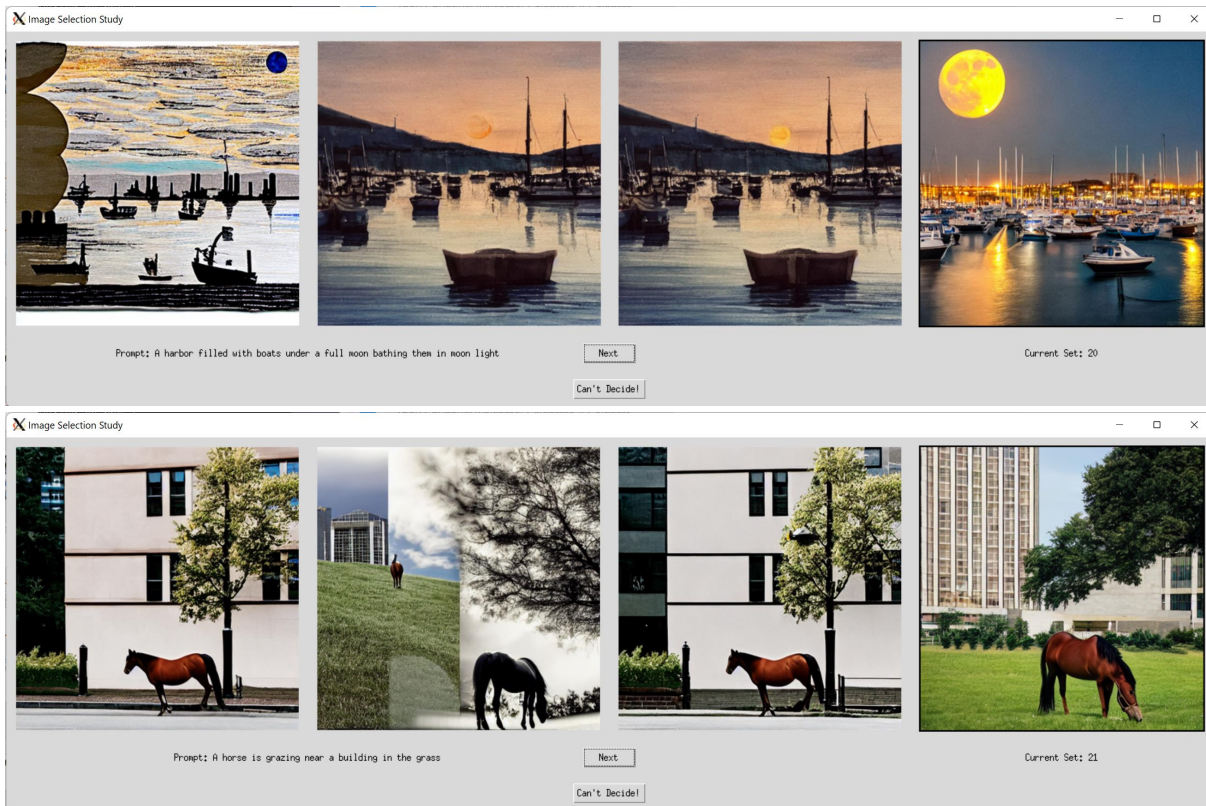


Figure 9: Human evaluation interface. See detailed results in the “Human Evaluation” subsection.